Published in final edited form as:
Neurobiol Aging. 2011 June ; 32(6): 1138–1148. doi:10.1016/j.neurobiolaging.2009.05.020.

Regional age-related effects in the monkey brain measured with ^{1}H magnetic resonance spectroscopy

Itamar Ronen[a,b,*], **Xiaoying Fan**[a], **Steve Schettler**[b], **Sahil Jain**[a,b], **Donna Murray**[b], **Dae-Shik Kim**[a,b], **Ronald Killiany**[a,b], and **Douglas Rosene**[b]

[a]Center for Biomedical Imaging, Boston University School of Medicine, Boston, MA 02118, USA

[b]Department of Anatomy and Neurobiology, Boston University School of Medicine, Boston, MA 02118, USA

Abstract

The rhesus monkey is a useful model for examining age-related effects on the brain, because of the extensive neuroanatomical homology between the monkey and the human brain, the tight control for neurological diseases as well as the possibility of obtaining relevant behavioral data and post-mortem tissue for histological analyses.

Here, proton magnetic resonance spectroscopy (^{1}H-MRS) was used together with high resolution anatomical MRI images to carefully assess regional concentrations of brain metabolites in a group of 20 rhesus monkeys.

In an anterior volume of interest (VOI) that covered frontal and prefrontal areas, significant positive correlations of myo-inositol and of total creatine concentrations with age were detected, whereas N-acetyl aspartate (NAA) and choline compounds (Cho) were not significantly correlated with age. In an occipito-parietal VOI, all metabolites showed no statistically significant age-dependent trend.

Strong correlations were found between NAA concentration and gray matter fraction in the VOIs as well as between choline compounds and white matter fraction.

Keywords

Magnetic Resonance Spectroscopy; Aging Brain; Rhesus monkey; Brain Metabolites

1. Introduction

Normal aging is associated with a vast array of physiological, structural and neurochemical changes in the brain that ultimately result in some level of cognitive and functional decline. The advent of non-invasive imaging and spectroscopic tools has made it possible to investigate these processes in a non-invasive manner, both in cross-section studies as well as

[*]Corresponding Author: Itamar Ronen, Ph.D. Department of Anatomy and Neurobiology 715 Albany Street L-1004 Boston University School of Medicine Boston MA 02118 Phone: 1-617-414-2360; Fax: 1-617-414-2371; Email: Itamar@bu.edu.

7. Disclosure None of the authors on this manuscript has any actual or potential conflict of interest pertinent to this work.

in longitudinal ones. Magnetic resonance spectroscopy (MRS) is a non-invasive tool that can be utilized to measure the presence and concentration of certain metabolites in living tissue at the millimolar concentration level. Several works have reported age-related effects on metabolite concentrations in frontal and prefrontal areas of the human brain as measured by magnetic resonance spectroscopy (MRS). Earlier single volume-of-interest (SV) MRS measurements (Chang et al. 1996; Soher et al. 1996; Pfefferbaum et al. 1999; Saunders et al. 1999; Leary et al. 2000) reported no significant age effects on N-acetyl Aspartate (NAA), a metabolite associated with neuronal viability, and a positive correlation with age in the concentration of choline compounds (Cho), whose increase is typically attributed to myelin degeneration and cell membrane breakdown. A later work (Brooks et al. 2001) included tissue parcellation analysis and the age-related effects on cerebrospinal fluid (CSF) volume in the quantification of the MRS data, and reported a negative correlation of frontal NAA levels with age, whereas the Cho and total creatine and phosphocreatine concentrations (tCr) did not significantly correlate with age (creatine is considered to be a global measure of brain energetics). Additional works showed similar trends (Lundbom et al. 1999; Kadota et al. 2001; Schuff et al. 2001), whereas others found no significant spectroscopic age-related changes in NAA concentration in gray matter, leading to the belief that neuronal viability in gray matter is resistant to aging (Adalsteinsson et al. 2000). SV-MRS with short echo time (TE) reveals more complex spectral information, and allows the quantification of more metabolites. Using short TE SV-MRS, it has been shown that glutamine and glutamate concentrations in the motor cortex correlated well with NAA and correlated negatively with age (Kaiser et al. 2005). In the same study it was shown that the white matter concentration of myoinositol (MI), a glial marker mostly present in astrocytes (Brand et al. 1993), exhibited positive correlation with age.

A recent meta-analysis of age-related MRS studies in humans was recently published in this journal (Haga et al. 2007) and the diversity of results obtained in the MRS studies surveyed in this work underscores the difficulty in inferring on age-related processes from human MRS data. This large range of MRS results stems from a variety of reasons, such as various levels of sophistication in the data analysis, but one of the main sources of inhomogeneity in the results is a concomitant inhomogeneity of the sampled cohort. Differences in life styles, overall health and genetic make-up of participants in human studies are likely to affect the variance of correlates of aging, and the variance is expected to increase with age.

Of the several alternative models used for aging research, the non-human primate model for aging and age-related changes in the brain is a particularly attractive one for several reasons. The extended homology between the monkey and the human brains makes it possible to make cross-species inferences both about brain neurophysiology and neuroanatomy as well as about behavioral trends that can be tested in both species. Secondly, the ability to closely control for the individual history of subjects in a monkey population is in sharp contrast to the large variance in health conditions and life styles found in the human population, differences that inevitably have consequences on brain physiology. Moreover, the monkey brain is less susceptible to Alzheimer disease (AD) (Roth et al. 2004), which in the case of human studies are prone to become confounds in the study of normal aging. Finally, the monkey aging model allows for several research paths that are less available in human studies, such as wider access to post-mortem tissue and various in-vivo interventions that can be tested in the frame of age-related phenomena.

One of the attractive features of the non-human primate model is the neuroanatomical homology between frontal and prefrontal cortical areas between humans and non-human primates, which has been shown to be highly relevant to the study of behavioral deficits in executive functions in both species, including age-related deficits. The role of prefrontal cortex in cognitive tasks in the rhesus monkey model has been studied extensively through

lesions preformed on key areas in the frontal and prefrontal cortex (Mishkin 1957; Gross 1963; Butter and Doehrman 1968; Goldman and Rosvold 1970; Iversen and Mishkin 1970). Subsequently, age-related cognitive decline in the rhesus monkey has been linked with regional age-related processes that selectively affect areas in the frontal and prefrontal cortex associated with specific types of cognitive impairments (Presty et al. 1987; Rapp and Amaral 1989; Arnsten and Goldman-Rakic 1990; Bachevalier et al. 1991).

Although very few MRS studies in non-human primates were aimed at aging, the monkey model has been extremely useful for a variety of MRS studies concerned with neurochemical changes in the brain. MRS was applied to the investigation of neuropathology associated with simian immunodeficiency virus (Greco et al. 2002; Williams et al. 2005), a primate model of Parkinson disease (Brownell et al. 1998) and exposure to early-life stressors (Mathew et al. 2003). One MRS study used monkeys as a model for aging (Herndon et al. 1998) and showed an increase in the ratio of myo-insositol to total creatine (mI/tCr) in a frontal volume of interest.

In this study we focus on investigating the neurochemical correlate of normal aging of the non-human primate brain. We use a tightly controlled population of 20 monkeys to obtain carefully quantified age-related cross sectional MRS data and show for the first time a regional differentiation in age-related trajectories in metabolite concentrations in two different regions in the monkey brain: an anterior region that included frontal and pre-frontal cortical areas and the anterior parts of the corpus callosum, and a posterior region that included parts of the visual cortex. The results are then discussed in the frame of age-related changes as documented in the past in several detailed histological and immunohistochemical studies.

2. Materials and Methods

2.1 Animals and animal procedures

20 adult rhesus monkeys (11 males and 9 females), ages 6-27 years, (*Macaca Mulatta*) were used for this study. Monkeys that participated in this study had no history of invasive experimental manipulations. The selection criteria excluded any animals exposed experimentally to neuroactive drugs as well as any animals with a health history of any neurological symptoms. All animal procedures were approved by the Institutional Animal Care and Use Committee (IACUC) of Boston University School of Medicine. Table 1 shows the distribution of age/sex across the population. Monkeys were anesthetized with an initial dose of ketamine (10 mg/kg i.m.) and xylazine (0.05 mg/kg i.m.) and brought to the scanner. In the scanner, animals were put in a stereotactic MRI-compatible head holder specially designed to fit within the radiofrequency coil used for the experiment. Body temperature was measured prior to the experiment and immediately after the scan was over. A MRI-compatible pulse-oxymeter sensor supplied with the MRI scanner was positioned on the monkey's rear foot for continuous reading of heart rate, and a respiration belt was positioned under the monkey's abdomen for respiration rate reading. Ketamine and xylazine boosters were provided as needed throughout the experiment, typically once every 25 minutes.

2.2 Hardware

All experiments were performed on a 3T whole body Intera MRI scanner (Philips Medical Systems, Best, The Netherlands). Radiofrequency (RF) coil used for this experiment was the 6-channel synergy receive-only head coil, while RF transmission was done through the quadrature body coil. The six channels in the head coil were combined in quadrature mode.

2.3 MRI and MRS experiments

A short survey scan consisted of coronal/sagittal/axial stacks of 3 slices each (T_1 fast field-echo (T1FFE), repetition time and echo time (TR/TE)=9ms/3.5ms, 5mm thickness, 10mm separation) was followed by a sensitivity encoding (SENSE) reference scan.

High resolution T_1-weighted scans were performed with the following parameters: 3D T_1 turbo field-echo (3D-T1TFE), TR/TE=8ms/3ms, turbo factor = 200, inter-shot delay = 2800ms, magnetization preparation = inversion, no. of averages = 6, field of view = 130×155×155 mm^3, resolution = 0.6×0.6×0.6 mm^3. Total scan time = 45 minutes.

Single volume-of-interest (SV) MRS scans were performed as following: sequence used was point resolved spectroscopy (PRESS) with TR/TE=3500ms/38ms. Phase cycles = 16, no. of averages = 256. Water suppression was achieved with selective excitation (bandwidth=140Hz at the water resonance) and dephasing using gradients on 3 axes. Four outer volume suppression bands on the sagittal plane (width = 30mm, separation from VOI = 5mm) were applied to further minimize contamination from the scalp and other lipid-rich areas. A scan without water suppression (no. of averages = 8) was performed for water scaling of the metabolite peaks. Receiver gain values for all water suppressed spectra and non-water suppressed spectra were kept respectively constant to allow for reproducible water peak based scaling. VOI dimensions were 13mm anterior-posterior, 13mm dorsal-ventral and 25mm left-right for a total of 4.2 mm^3. The positioning of the VOIs in the anterior location and the posterior location was done as consistently as possible across monkeys. Figure 1 shows the location of the anterior VOI (panels a-c) and posterior VOI (panels d-f) on the sagittal, coronal and axial planes. Both VOIs were positioned symmetrically on the medio-lateral axis. The anterior VOI was pushed as anterior and as dorsal as possible with the dorsal face of the VOI parallel to the skull in the anterior-posterior direction (panel a), without allowing contaminations from the fat in the eye orbits (panel c) as well as from the scalp above the VOI lateral edges (panel b). This requirement, coupled with a relatively small variance in the brain size and shape across monkeys, allowed for a reliably reproducible positioning of the volume. Areas included in the anterior VOI are: anterior cingulate cortex, rostrum and genu of the corpus callosum, supplementary motor area (SMA) and parts of Brodmann area 46. The medio-lateral axis of the VOI was approximately 25mm dorsal and 32mm anterior to the Saleem-Logothetis reference planes (Saleem and Logothetis 2007), with a typical 15° forward tilt with respect to the vertical reference plane. The posterior VOI was positioned above the cerebellum and as posterior as possible, parallel to the skull in the anterior-posterior direction (panel d), excluding possible contamination from the posterior-dorsal edge of the VOI (panels e and f). Areas included in the posterior VOI are: early visual areas (e.g. V2, V3), area MT, and posterior areas of the medial-parietal cortex. Areas included in this VOI are not known to have an age-related behavioral outcome, although microstructural changes in occipital white matter have been studied (Peters et al. 2001). The medio-lateral axis of the VOI was approximately 28mm dorsal and 10mm posterior to the Saleem-Logothetis reference planes, with a typical 45° tilt with respect to the vertical reference plane. Total scan time = 45 minutes.

2.4 Data processing and analysis

MRI processing—MRI and MRS data were exported in Philips research format (PAR/REC and SDAT/SPAR, respectively). Image processing was performed using a C++ home-written multimodal MRI viewing and analysis tool, and MATLAB® (Mathworks, Natick MA). The high-resolution T_1-weighted images were skull-stripped and segmented into three tissue types: gray matter, white matter and CSF. The fully-automated segmentation was based on a combination of hidden Markov random field model and an associated

expectation-maximization algorithm (Zhang et al. 2001). Based on the segmentation results, three tissue-specific probability maps were generated for the three tissue types.

Figure 2 shows a coronal view of a T_1-weighted image of one of the monkeys (panel a), along with the segmentation results (panel b) and the three tissue probability maps for grey matter, white matter and CSF (panels c-e) generated from the segmentation. The coordinates/angulation values of the VOIs were used to generate a mask that includes all pixels that belong to the VOI. To avoid round-off errors generated by the arbitrary location and angulation of the VOI with respect to the image grid, the VOI mask was created as a probability map, where pixels that were fully within the VOI were given the probability p=1, pixels outside the VOI obtained p=0 and pixels "cut" by an edge of the VOI were given a probability value p proportional to the fraction of the pixel within the VOI. Figure 2f shows the intersection of the anterior VOI probability map with the gray matter probability map on the coronal plane. The tissue fractions within the VOI were calculated according to:

$$f_{tissue}=\frac{\sum_{n=1}^{N} p_{n,tissue}\cdot p_{n,VOI}}{\sum_{n=1}^{N} p_{n,VOI}}$$

Where f_{tissue} is the tissue fraction within the VOI and tissue is either gray matter, white matter or CSF, $p_{n,tissue}$ is the probability of a pixel n to belong to the tissue, and $p_{n,VOI}$ is the probability of the pixel n to belong to the VOI. The sum runs on all N pixels in the image.

MRS data processing—exported MRS data was analyzed using LCModel (www.s-provencher.com, Oakville, ON, CA, (Provencher 1993)). LCModel estimates metabolite concentration both as a fraction of the creatine/phosphocreatine peak (total creatine, or tCr), as well as against the spectrum of the water peak, obtained without water suppression. The resulting concentrations retain a certain amount of uncertainty with respect to actual concentrations and are thus given in "institutional units" (i.u.), but given a consistent experimental setting (similar VOIs, experimental parameters such as TR/TE of the PRESS sequence, RF coil, receiver gain), the inter-experimental stability of the LCModel i.u. output is extremely high and is used as the "gold standard" for quantification of in-vivo proton MRS data. The i.u. values for the metabolites of interest (NAA, tCr, Cho and MI) were further corrected to the contribution of CSF, where the metabolite concentration is negligible. The correction is thus performed according to:

$$C_{corr.}=C_{LCModel}\cdot\frac{1}{1-f_{csf}}$$

Where $C_{corr.}$ is the corrected metabolite concentration, $C_{LCModel}$ is the water-scaled metabolite concentration provided by the LCModel calculation and f_{CSF} is the fraction of the CSF in the VOI. Statistical analyses were performed using SPSS v. 16 (SPSS inc., Chicago, IL).

All data sets acquired (N=20) were used for the analysis of the frontal VOI, and one was discarded from the analysis of the posterior VOI because of segmentation errors in the occipital pole/cerebellar area, leaving N=19 for posterior VOI data. Analyses of age and tissue type effects on metabolite concentrations were bivariate Pearson's correlations (two-tailed).

3. Results

3.1 tissue content and tissue fraction analysis

The tissue probability maps obtained from the tissue segmentation results were used to calculate the gray matter, white matter and CSF fractions within each VOI. The graphs in figures 3a and 3b show the correlation of tissue fractions within the anterior and posterior VOIs with age. Within each VOI the variance of all three tissue fractions was about 10% of the corresponding tissue fraction, attesting for the good reproducibility of the VOI positioning. A summary of the tissue fraction findings within the VOIs is given in table 2.

3.2 MRS results

This study aimed at the quantitative assessment of four metabolites: N-acetyl aspartate (NAA) is co-measured with N-acetyl aspartyl glutamate (NAAG), and for simplicity will be referred to as NAA. Soluble choline compounds - phosphocholine and glycerophosphocholine - are denoted as Cho. The total creatine content (creatine and phoshphocreatine) is denoted by tCr and myo-inositol with MI. Figure 4 shows typical anterior VOI spectra for two monkeys, one of age 8.4 years and the other of age 24.4 years. The solid line overlaid on the spectrum represents the LCModel fit. Actual concentrations (in i.u.) for NAA, tCr, Cho and MI in these spectra are given in the figure caption. The average standard deviation for the individual metabolite concentration measurement in percent of the measured value, as derived from the Cramer-Rao lower bound (CRLB) for the measurement, was 4% for NAA, 3% for tCr, 8% for MI and 7% for Cho.

Figure 5a shows the concentrations of NAA and Cho in the frontal VOI, corrected for CSF fraction in the VOI, vs. age. Figure 5b shows the corrected concentrations of MI and tCr vs. age. The separation in two graphs is for visual clarity. Both MI and tCr are significantly correlated with age in the anterior VOI, while NAA and Cho show less than significant correlation with age. Figures 5c and 5d show the concentrations of NAA and Cho (5c) and those of MI and tCr (5d) in the posterior VOI versus age. No significant correlation has been found for any of the four metabolites with age in the posterior region, although the NAA shows a negative trend with age ($r=-0.38$, $p=0.11$). The complete statistical analysis of the metabolite concentrations in both VOIs, including the slopes of the linear regressions and their standard errors (S.E.), is given in table 3. Separate analyses for age-related effects on metabolite concentrations in the subgroups of 11 females and 9 males are given in table 4.

It can be seen that the individual variability of the NAA concentration across subjects is non-negligible, despite the very small individual standard deviation in the NAA measurement, expressed by the Cramer-Rao lower bound estimate, which for the NAA measurements was typically about 2%. In particular, there is a significant difference between the average concentration of NAA in the anterior VOI and in the posterior one. The tissue composition of both VOIs is significantly different, and in particular in their gray matter to white matter ratios. For this reason, the spectroscopic results for each metabolite within the two volumes were grouped together and the possibility of correlation between tissue type and metabolite was explored. Third and fourth columns in table 3 show the Pearson's correlation coefficients and the corresponding p values for the correlations between the concentration of all four metabolites (corrected for CSF) and the fractions of gray and white matter in the VOI. The NAA concentration was positively correlated with the gray matter fraction in the VOI, and the Cho concentration correlated well with the white matter fraction (and negatively with the gray matter fraction). MI and tCr concentrations showed no correlation with any tissue type. No significant correlations were found between any metabolite concentration in the anterior VOI and the concentration in the posterior one

in the same monkey (last column in table 3). Figure 6 shows the correlation of NAA and Cho (6a) and that of tCr and MI (6b) with gray matter fraction for all measurements.

4. Discussion

In the frontal VOI, two of the four metabolites showed a significant correlation with age. Myo-inositol (MI), an osmolyte highly present in astrocytes (Brand et al. 1993), was shown to be significantly positively correlated with age. This is in agreement with previous studies both in monkeys and humans (Herndon et al. 1998; Saunders et al. 1999; Ross et al. 2006). In particular, a longitudinal study on healthy elderly humans showed that over the range of three years, the concentration of MI in frontal white matter significantly increased (Ross et al. 2006), but no correlation with neurophysiological function was found. Further corroboration to the connection between the frontal increase in MI and age-related processes that mainly affect white matter was given by immunohistochemistry (Sloane et al. 2000), where white-matter specific astrocytic hypertrophy was found in frontal, temporal and parietal areas of post-mortem rhesus monkey brains, with no concomitant increases in gray matter astrocytic hypertrophy were found in the examined areas. Ross et al. hypothesized that increasing MI may be a marker of aging or a preclinical neurodegenerative process. Here there is corroborative evidence for the link with aging, but in the rhesus model it is most likely that the link with preclinical neurodegeneration can be excluded. Myo-inositol concentration in the anterior VOI also positively correlated with age in the males and females subgroups with similar correlation coefficient ($r \approx 0.5$ for both sexes) but the statistical significance of this trend was low ($p=0.12$ for females and $p=0.15$ for males).

The increase in tCr in the anterior VOI with age is significant, and similar increases were found in some of the human MRS aging studies in frontal regions (McIntyre et al. 2007) but not in others (Brooks et al. 2001). An age-related decrease in creatine kinase activity has been reported in humans and rats, as measured with ^{31}P-NMR (Smith et al. 1997) and it is possible that age-related increased tCr is associated with reduction in energetic capability of brain cells with age. The age-related increase in tCr, as found in this study and others, emphasizes the importance of water-based quantification of metabolite concentration in *in vivo* MRS, rather than relative quantification with respect to the tCr level. Anterior tCr was significantly correlated with age in the group of females ($p=0.02$) but not in the group of males ($p=0.28$).

In neither VOI was there a highly significant correlation of NAA concentration with age. The meta-analysis of age-related MRS studies in humans mentioned earlier (Haga et al. 2007) reports that 5 out of 8 studies show no change in frontal NAA concentrations (with one showing increase and two studies showing decrease), whereas occipital NAA concentrations were rarely studied - one study showed decrease in occipital NAA and one shows no change. In this study, the NAA concentration in the anterior VOI showed no significant age-related trend, whereas that in the posterior VOI showed a less-than-significant decrease with age ($r=-0.38$, $p=0.11$). This decrease becomes significant when the results obtained from group of 9 male monkeys are separately analyzed (see table 4). With such a low number of monkeys and a highly inhomogeneous distribution of ages in this particular group, these results call for further corroboration with more data from middle-aged and older monkeys. It has been previously shown that in the rhesus monkey brain there is a thinning of cortical layer 1 both in Brodmann area 46 in the prefrontal cortex (Peters et al. 1998) as well as in the visual cortex (Peters et al. 2001), a thinning that is not associated with loss in neurons. The finding in this work that NAA is not significantly correlated with age in the frontal VOI when the data obtained from the entire population is analyzed may support the notion of resistance of gray matter neurons in frontal gray matter to healthy aging, and that significant age-related morphometric changes in gray matter in such areas,

e.g. (Alexander et al. 2008) result from changes in other constituents rather than the total number of neurons, although the mechanism underlying these changes still remains unclear.

Regional differences in age-effects on the concentration of metabolites measured in this study can also be assessed by examining the difference in slopes ([metabolite]/age) of the linear regression results obtained from the two VOIs, as they are given in Table 2. As expected, differences are seen between the slope of [MI]/age and [tCr]/age between the two VOIs, although the standard errors for the slopes are too large for the differences to be determined as statistically significant, as they are less than two S.E. apart from each other. Interestingly, the slope of [NAA]/age in the anterior VOI and that in the posterior VOI are more than one S.E. apart from each other. Although this does not reach the level of statistical significance, and neither does any of linear regressions for [NAA]/age in either VOI, this finding, taken with the almost significant negative trend ($r=-0.38$ $p=0.11$) of NAA concentration in the posterior VOI, could be indicative of differences in regional age effects on NAA concentration, although further corroboration is needed.

It should be noted that the accuracy of the estimation of the metabolite concentrations in this study is limited by the inability to obtain MRS data from VOIs with a single tissue type (GM or WM). The added variance is due to the different amounts of MR-visible water in GM and WM, and when the VOI contains only one tissue type and CSF, it is possible to model the tissue water content in the quantification of the metabolites, as done e.g. in (Brooks et al. 2001). The confidence in the age effect on MI and tCr concentrations in the frontal VOI is increased, however, thanks to the fact that no age effect on tissue type was observed in either VOIs.

Although the spatial resolution of the MRS measurement (4.2cc) was not sufficient to selectively place the VOIs on gray matter and white matter areas, it was shown that segmentation data from high-resolution, high-contrast anatomical images that are co-registered with the VOI coordinates can help generate reliable information about the distribution of metabolites across tissue types. Higher prevalence of certain metabolites in specific brain tissue type has been reported in human MRS studies, and is for the most part in accordance with what this study reports. Higher NAA concentration in gray matter (Christiansen et al. 1993; Charles et al. 1994; Chang et al. 1996; Saunders et al. 1999) and higher Cho concentration in white matter (May et al. 1986; Barker et al. 1993) were previously reported. In this study, as well as in other studies (Michaelis et al. 1991; Christiansen et al. 1993) the MI concentration did not seem to be tissue-preferential.

5. Conclusions and Future Studies

It is shown here that MRS in combination with tissue segmentation can be used to investigate regional age effects on metabolite concentrations in the rhesus monkey model for the aging brain. The results shown here are in good agreement with some of the findings reported from post-mortem tissue analyses, e.g. increase in $GFAP^+$ in frontal and parietal white matter (Sloane et al. 2000) and the cortical thinning that was unaccompanied by significant decline in neuronal count in gray matter areas (Peters et al. 1998). The relationship between the neuroanatomical changes detected in post-mortem tissue and age-related MRS findings has to be further more robustly cross-validated by studies that provide MRS/MRI data, histological data and immunohistochemical data from the same group of monkeys.

One of the shortcomings of this study is the limited number of metabolites that could be accurately assessed without confounds. A recent MRS study in humans showed regional age-related changes in glutamate, an excitatory neurotransmitter (Kaiser et al. 2005). Data for glutamate concentrations were available in this study, but the reliability of these

measurements is confounded by the use of ketamine as the anesthetic agent, and the effect that ketamine has on glutamate metabolism (Rowland et al. 2005). Thus, a different anesthesia protocol is needed for the exploration of regional changes in glutamine/glutamate concentrations.

Single VOI MRS has the distinct advantage of allowing simple and robust quantification of the metabolites in the volume. The implementation of MR spectroscopic imaging (MRSI) in future studies will allow, on the other hand, larger area coverage and further insight into the tissue preferentiality of brain metabolites, as has been shown in human age-related MRSI studies (Pfefferbaum et al. 1999; Schuff et al. 1999; Schuff et al. 2001).

Acknowledgments

This work is supported by NIH grants P01-AG000001-31 and R21-AG028781.

References

Adalsteinsson E, Sullivan EV, Kleinhans N, Spielman DM, Pfefferbaum A. Longitudinal decline of the neuronal marker N-acetyl aspartate in Alzheimer's disease. Lancet. 2000; 355(9216):1696–7. [PubMed: 10905250]

Alexander GE, Chen K, Aschenbrenner M, Merkley TL, Santerre-Lemmon LE, Shamy JL, Skaggs WE, Buonocore MH, Rapp PR, Barnes CA. Age-related regional network of magnetic resonance imaging gray matter in the rhesus macaque. J Neurosci. 2008; 28(11):2710–8. [PubMed: 18337400]

Andersen AH, Zhang Z, Zhang M, Gash DM, Avison MJ. Age-associated changes in rhesus CNS composition identified by MRI. Brain Res. 1999; 829(1-2):90–8. [PubMed: 10350533]

Arnsten AF, Goldman-Rakic PS. Analysis of alpha-2 adrenergic agonist effects on the delayed nonmatch-to-sample performance of aged rhesus monkeys. Neurobiol Aging. 1990; 11(6):583–90. [PubMed: 1980719]

Bachevalier J, Lnandis LS, Walker LC, Brickson M, Mishkin M, Price DL, Cork LC. Aged monkeys exhibit behavioral deficits indicative of widespread cerebral dysfunction. Neurobiol Aging. 1991; 12(2):99–111. [PubMed: 2052134]

Barker PB, Soher BJ, Blnackband SJ, Chatham JC, Mathews VP, Bryan RN. Quantitation of proton NMR spectra of the human brain using tissue water as an internal concentration reference. NMR Biomed. 1993; 6(1):89–94. [PubMed: 8384470]

Brand A, Richter-Lnandsberg C, Leibfritz D. Multinuclear NMR studies on the energy metabolism of glial and neuronal cells. Dev Neurosci. 1993; 15(3-5):289–98. [PubMed: 7805581]

Brooks JC, Roberts N, Kemp GJ, Gosney MA, Lye M, Whitehouse GH. A proton magnetic resonance spectroscopy study of age-related changes in frontal lobe metabolite concentrations. Cereb Cortex. 2001; 11(7):598–605. [PubMed: 11415962]

Brownell AL, Jenkins BG, Elmaleh DR, Deacon TW, Spealman RD, Isacson O. Combined PET/MRS brain studies show dynamic and long-term physiological changes in a primate model of Parkinson disease. Nat Med. 1998; 4(11):1308–12. [PubMed: 9809556]

Butter CM, Doehrman SR. Size discrimination and transposition in monkeys with striate and temporal lesions. Cortex. 4(1). 1968; 4(1):35–45.

Chang L, Ernst T, Polnand RE, Jenden DJ. In vivo proton magnetic resonance spectroscopy of the normal aging human brain. Life Sci. 1996; 58(22):2049–56. [PubMed: 8637436]

Charles HC, Lnazeyras F, Krishnan KR, Boyko OB, Patterson LJ, Doraiswamy PM, McDonald WM. Proton spectroscopy of human brain: effects of age and sex. Prog Neuropsychopharmacol Biol Psychiatry. 1994; 18(6):995–1004. [PubMed: 7824764]

Christiansen P, Toft P, Lnarsson HB, Stubgaard M, Henriksen O. The concentration of N-acetyl aspartate, creatine + phosphocreatine, and choline in different parts of the brain in adulthood and senium. Magn Reson Imaging. 1993; 11(6):799–806. [PubMed: 8371635]

Goldman PS, Rosvold HE. Localization of function within the dorsolateral prefrontal cortex of the rhesus monkey. Exp Neurol. 1970; 27(2):291–304. [PubMed: 4987453]

Grachev ID, Apkarian AV. Aging alters regional multichemical profile of the human brain: an in vivo 1H-MRS study of young versus middle-aged subjects. J Neurochem. 2001; 76(2):582–93. [PubMed: 11208921]

Greco JB, Sakaie KE, Aminipour S, Lee PL, Chang LL, He J, Westmorelnand S, Lnackner AA, Gonzalez RG. Magnetic resonance spectroscopy: an in vivo tool for monitoring cerebral injury in SIV-infected macaques. J Med Primatol. 2002; 31(4-5):228–36. [PubMed: 12390545]

Gross CG. Locomotor activity following lateral frontal lesions in rhesus monkeys. J Comp Physiol Psychol. 1963; 56:232–6. [PubMed: 13950748]

Haga KK, Khor YP, Farrall A, Wardlnaw JM. A systematic review of brain metabolite changes, measured with (1)H magnetic resonance spectroscopy, in healthy aging. Neurobiol Aging. 2007

Herndon JG, Constantinidis I, Moss MB. Age-related brain changes in rhesus monkeys: a magnetic resonance spectroscopic study. Neuroreport. 1998; 9(9):2127–30. [PubMed: 9674606]

Iversen SD, Mishkin M. Perseverative interference in monkeys following selective lesions of the inferior prefrontal convexity. Exp Brain Res. 1970; 11(4):376–86. [PubMed: 4993199]

Kadota T, Horinouchi T, Kuroda C. Development and aging of the cerebrum: assessment with proton MR spectroscopy. AJNR Am J Neuroradiol. 2001; 22(1):128–35. [PubMed: 11158898]

Kaiser LG, Schuff N, Cashdollnar N, Weiner MW. Age-related glutamate and glutamine concentration changes in normal human brain: 1H MR spectroscopy study at 4 T. Neurobiol Aging. 2005; 26(5): 665–72. [PubMed: 15708441]

Leary SM, Brex PA, MacManus DG, Parker GJ, Barker GJ, Miller DH, Thompson AJ. A (1)H magnetic resonance spectroscopy study of aging in parietal white matter: implications for trials in multiple sclerosis. Magn Reson Imaging. 2000; 18(4):455–9. [PubMed: 10788723]

Lundbom N, Barnett A, Bonavita S, Patronas N, Rajapakse J, Tedeschi, Di Chiro G. MR image segmentation and tissue metabolite contrast in 1H spectroscopic imaging of normal and aging brain. Magn Reson Med. 1999; 41(4):841–5. [PubMed: 10332862]

Makris N, Papadimitriou GM, van der Kouwe A, Kennedy DN, Hodge SM, Dale AM, Benner T, Wald LL, Wu O, Tuch DS, Caviness VS, Moore TL, Killiany RJ, Moss MB, Rosene DL. Frontal connections and cognitive changes in normal aging rhesus monkeys: a DTI study. Neurobiol Aging. 2007; 28(10):1556–67. [PubMed: 16962214]

Mathew SJ, Shungu DC, Mao X, Smith EL, Perera GM, Kegeles LS, Perera T, Lisanby SH, Rosenblum LA, Gorman JM, Coplnan JD. A magnetic resonance spectroscopic imaging study of adult nonhuman primates exposed to early-life stressors. Biol Psychiatry. 2003; 54(7):727–35. [PubMed: 14512213]

May GL, Wright LC, Holmes KT, Williams PG, Smith IC, Wright PE, Fox RM, Mountford CE. Assignment of methylene proton resonances in NMR spectra of embryonic and transformed cells to plasma membrane triglyceride. J Biol Chem. 1986; 261(7):3048–53. [PubMed: 3949759]

McIntyre DJ, Charlton RA, Markus HS, Howe FA. Long and short echo time proton magnetic resonance spectroscopic imaging of the healthy aging brain. J Magn Reson Imaging. 2007; 26(6): 1596–606. [PubMed: 17968966]

Michaelis T, Merboldt KD, Hanicke W, Gyngell ML, Bruhn H, Frahm J. On the identification of cerebral metabolites in localized 1H NMR spectra of human brain in vivo. NMR Biomed. 1991; 4(2):90–8. [PubMed: 1677588]

Mishkin M. Effects of small frontal lesions on delayed alternation in monkeys. J Neurophysiol. 1957; 20(6):615–22. [PubMed: 13476217]

Peters A, Moss MB, Sethares C. Effects of aging on myelinated nerve fibers in monkey primary visual cortex. J Comp Neurol. 2000; 419(3):364–76. [PubMed: 10723011]

Peters A, Moss MB, Sethares C. The effects of aging on layer 1 of primary visual cortex in the rhesus monkey. Cereb Cortex. 2001; 11(2):93–103. [PubMed: 11208664]

Peters A, Sethares C. Aging and the myelinated fibers in prefrontal cortex and corpus callosum of the monkey. J Comp Neurol. 2002; 442(3):277–91. [PubMed: 11774342]

Peters A, Sethares C, Killiany RJ. Effects of age on the thickness of myelin sheaths in monkey primary visual cortex. J Comp Neurol. 2001; 435(2):241–8. [PubMed: 11391644]

Peters A, Sethares C, Moss MB. The effects of aging on layer 1 in area 46 of prefrontal cortex in the rhesus monkey. Cereb Cortex. 1998; 8(8):671–84. [PubMed: 9863695]

Pfefferbaum A, Adalsteinsson E, Spielman D, Sullivan EV, Lim KO. In vivo spectroscopic quantification of the N-acetyl moiety, creatine, and choline from large volumes of brain gray and white matter: effects of normal aging. Magn Reson Med. 1999; 41(2):276–84. [PubMed: 10080274]

Presty SK, Bachevalier J, Walker LC, Struble RG, Price DL, Mishkin M, Cork LC. Age differences in recognition memory of the rhesus monkey (Macaca mulatta). Neurobiol Aging. 1987; 8(5):435–40. [PubMed: 3683724]

Provencher SW. Estimation of metabolite concentrations from localized in vivo proton NMR spectra. Magn Reson Med. 1993; 30(6):672–9. [PubMed: 8139448]

Rapp PR, Amaral DG. Evidence for task-dependent memory dysfunction in the aged monkey. J Neurosci. 1989; 9(10):3568–76. [PubMed: 2795141]

Ross AJ, Sachdev PS, Wen W, Brodaty H. Longitudinal changes during aging using proton magnetic resonance spectroscopy. J Gerontol A Biol Sci Med Sci. 2006; 61(3):291–8. [PubMed: 16567380]

Roth GS, Mattison JA, Ottinger MA, Chachich ME, Lnane MA, Ingram DK. Aging in rhesus monkeys: relevance to human health interventions. Science. 2004; 305(5689):1423–6. [PubMed: 15353793]

Rowland LM, Bustillo JR, Mullins PG, Jung RE, Lenroot R, Lnandgraf E, Barrow R, Yeo R, Lnauriello J, Brooks WM. Effects of ketamine on anterior cingulate glutamate metabolism in healthy humans: a 4-T proton MRS study. Am J Psychiatry. 2005; 162(2):394–6. [PubMed: 15677610]

Saleem, KS.; Logothetis, NK. Atlas of the Rhesus Monkey Brain in Stereotaxic Coordinates. Academic Press; 2007.

Saunders DE, Howe FA, van den Boogaart A, Griffiths JR, Brown MM. Aging of the adult human brain: in vivo quantitation of metabolite content with proton magnetic resonance spectroscopy. J Magn Reson Imaging. 1999; 9(5):711–6. [PubMed: 10331768]

Schuff N, Amend DL, Knowlton R, Norman D, Fein G, Weiner MW. Age-related metabolite changes and volume loss in the hippocampus by magnetic resonance spectroscopy and imaging. Neurobiol Aging. 1999; 20(3):279–85. [PubMed: 10588575]

Schuff N, Ezekiel F, Gamst AC, Amend DL, Capizzano AA, Maudsley AA, Weiner MW. Region and tissue differences of metabolites in normally aged brain using multislice 1H magnetic resonance spectroscopic imaging. Magn Reson Med. 2001; 45(5):899–907. [PubMed: 11323817]

Sloane JA, Hollnander W, Rosene DL, Moss MB, Kemper T, Abraham CR. Astrocytic hypertrophy and altered GFAP degradation with age in subcortical white matter of the rhesus monkey. Brain Res. 2000; 862(1-2):1–10. [PubMed: 10799662]

Smith CD, Lnandrum W, Carney JM, Lnandfield PW, Avison MJ. Brain creatine kinase with aging in F-344 rats: analysis by saturation transfer magnetic resonance spectroscopy. Neurobiol Aging. 1997; 18(6):617–22. [PubMed: 9461059]

Soher BJ, van Zijl PC, Duyn JH, Barker PB. Quantitative proton MR spectroscopic imaging of the human brain. Magn Reson Med. 1996; 35(3):356–63. [PubMed: 8699947]

Williams K, Westmoreland S, Greco J, Ratai E, Lentz M, Kim WK, Fuller RA, Kim JP, Autissier P, Sehgal PK, Schinazi RF, Bischofberger N, Piatak M, Lifson JD, Masliah E, Gonzalez RG. Magnetic resonance spectroscopy reveals that activated monocytes contribute to neuronal injury in SIV neuro AIDS. J Clin Invest. 2005; 115(9):2534–2545. [PubMed: 16110325]

Zhang Y, Brady M, Smith S. Segmentation of brain MR images through a hidden Markov random field model and the expectation-maximization algorithm. IEEE Trans Med Imaging. 2001; 20(1): 45–57. [PubMed: 11293691]

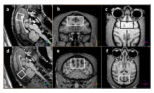

Figure 1.
Typical anterior VOI (panels a-c) and posterior VOI (panels d-f) in sagittal (a,d), coronal (b,e) and axial (c,f) views. Views are defined by the MRI coordinates and thus not parallel to the VOIs sides.

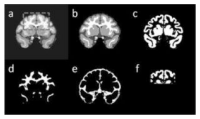

Figure 2.
(a) coronal view of a skull-stripped T_1-weighted image. The contours of the anterior VOI are marked in dashed gray line; (b) segmentation results of the same slice. Dark gray: CSF, light gray: gray matter, white: white matter; (c) same slice - gray matter probability map; (d) white matter probability map; (e) CSF probability map; (f) intersection between the gray matter probability map and the VOI.

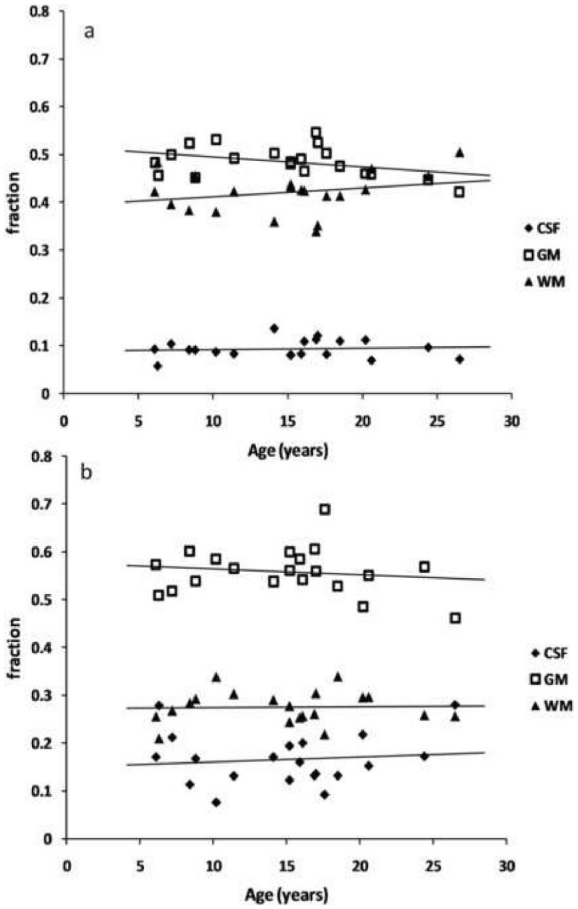

Figure 3.
Tissue fractions in (a) the anterior VOI and (b) the posterior VOI against age. GM: gray matter, WM: white matter, CSF: cerebrospinal fluid.

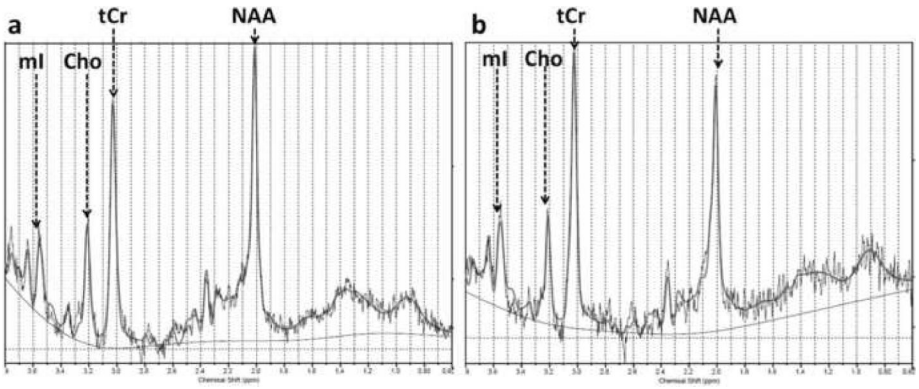

Figure 4.

Typical anterior VOI MRS spectra taken from (a) a 8.4 year old and (b) a 24.4 year old monkey. The actual concentrations in i.u. for the spectrum in (a) are: NAA=9.15 i.u., Cho=1.67 i.u., tCr=11.16 i.u., MI=6.60 i.u., and for the spectrum in (b): NAA=9.04 i.u., Cho=1.47 i.u., tCR=12.98 i.u. and MI=9.3 i.u.

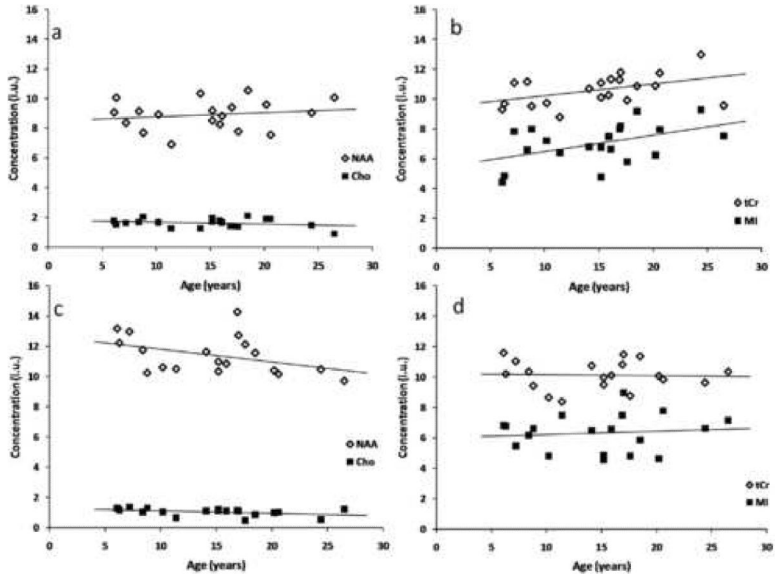

Figure 5.

Metabolite concentrations vs. age in the anterior VOI (panels a,b) and in the posterior VOI (panels c,d). Concentrations are given in institutional units (i.u.). MI and tCr in the anterior VOI showed significant positive correlation with age, and NAA in the posterior VOI exhibited a less-than-significant negative trend.

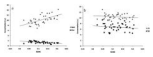

Figure 6.
Metabolite concentrations vs. gray matter fraction, f(GM), for all measurements. The metabolites that showed the most significant correlation with tissue type were NAA, which positively correlated with f(GM) and Cho, which negatively correlated with f(GM) and positively with the white matter fraction. tCr and MI were not significantly correlated with either tissue type.

Table1

Monkey population data

identifier	sex	Age(y)
M1	M	6.1
M2	M	6.3
M3	M	7.2
M4	M	8.4
M5	M	8.8
M6	M	10.2
M7	F	11.4
M8	F	14.1
M9	M	15.2
M10	M	15.2
M11	F	15.9
M12	F	16.1
M13	F	16.9
M14	F	17.0
M15	F	17.6
M16	F	18.5
M17	M	20.2
M18	F	20.6
M19	M	24.4
M20	M	26.5

Table 2

Anterior VOI, posterior VOI statistical analysis results.

	Mean (St. Dev.)	**Mean (St. Dev.)**
	Correlation with age (Anterior VOI) N=20	**Correlation with age (Posterior VOI) N=19**
f_{GM}	0.49 (0.03)	0.56 (0.05)
	r=-0.38, p=0.10	r=-0.19, p=0.43
f_{WM}	0.42 (0.04)	0.28 (0.03)
	r=0.25, p=0.29	r=-0.01, p=0.96
f_{CSF}	0.09 (0.02)	0.17 (0.05)
	r=0.08, p=0.75	r=0.15, p=0.53

r = Pearson's correlation coefficient.

Table 3

MRS statistical analysis results: metabolite group statistics, correlation with age, tissue type and VOI location.

	Concentration (i.u.) Mean (St. Dev.) **Correlation with age (anterior VOI) N=20** **Slope (i.u./year) (S.E.)**	**Concentration (i.u.) Mean (St. Dev.)** **Correlation with age (posterior VOI) N=19** **Slope (i.u./year) (S.E.)**	**Correlation with f_{GM} (both VOIs) N=39**	**Correlation with f_{WM} (both VOIs) N=39**	**Correlation Between VOIs N=19**
NAA	9.11 (1.29)	11.41 (1.24)			
	r=0.18, p=0.44	r=-0.38, p=0.11	***r=0.60, p<0.001***	***r=-0.71, p<0.001(**)***	r=0.02, p=0.95
	0.03 (0.04)	-0.08 (0.04)			
Cho	1.62 (0.3)	1.06 (0.24)			
	r=-0.24, p=0.31	r=-0.36, p=0.13	***r=-0.62, p<0.001***	***r=0.66, p<0.001(**)***	r=0.18, p=0.47
	-0.01 (0.01)	-0.02 (0.01)			
MI	***7.00 (1.35)***	6.32 (1.22)			
	r=0.47, p=0.03(*)	r=0.13, p=0.59	r=-0.25, p=0.15	r=0.20, p=0.215	r=-0.13, p=0.61
	0.11 (0.05)	0.02 (0.04)			
tCr	***10.60 (1.02)***	10.12 (0.94)			
	r=0.45, p=0.04(*)	r=0.02, p=0.95	r=-0.28, p=0.1	r=0.16, p=0.345	r=0.31, p=0.2
	0.079 (0.04)	-0.01 (0.04)			

Table 4

MRS statistical analysis results (separate analyses for males and females).

	Concentration (i.u.) Mean (St. Dev.)	**Concentration (i.u.) Mean (St. Dev.)**	**Concentration (i.u.) Mean (St. Dev.)**	**Concentration (i.u.) Mean (St. Dev.)**
	Correlation with age (anterior VOI) Females (N=11)	**Correlation with age (posterior VOI) Females (N=10)**	**Correlation with age (anterior VOI) Males (N=9)**	**Correlation with age (posterior VOI) Males (N=9)**
NAA	8.74 (1.17)	11.52 (1.27)	9.11 (0.76)	***11.29 (1.28)***
	r=0.13, p=0.72	r=.154, p=0.672	r=0.40, p=0.28	***r=-0.74, p=0.02(*)***
Cho	1.62 (0.3)	1.00 (0.24)	1.62 (0.32)	1.12 (0.25)
	r=0.529, p=0.09	r=0.03, p=0.92	r=-0.56, p=0.12	r=-0.55, p=0.13
MI	7.1 (1.24)	6.49 (1.47)	6.89 (1.56)	6.13 (0.92)
	r=0.50, p=0.12	r=0.10, p=0.78	r=0.52, p=0.15	r=0.08, p=0.84
tCr	***10.72 (0.89)***	10.09 (1.04)	10.44 (1.20)	10.15 (0.87)
	r=0.69, p=0.02(*)	r=0.39, p=0.27	r=0.41, p=0.28	r=-0.23, p=0.56